Retention and entrainment effects: Experiments and theory for porous spheres settling in sharply stratified fluids

R. Camassa, S. Khatri, R. M. McLaughlin, J. C. Prairie, B. L. White et al.

Additional information on Phys. Fluids

Journal Homepage: http://pof.aip.org/
Journal Information: http://pof.aip.org/about/about_the_journal
Top downloads: http://pof.aip.org/features/most_downloaded
Information for Authors: http://pof.aip.org/authors

Retention and entrainment effects: Experiments and theory for porous spheres settling in sharply stratified fluids

R. Camassa,[1] S. Khatri,[1,a)] R. M. McLaughlin,[1] J. C. Prairie,[1,2] B. L. White,[2] and S. Yu[2]
[1]*Carolina Center for Interdisciplinary Applied Mathematics, Department of Mathematics, University of North Carolina at Chapel Hill, Chapel Hill, North Carolina 27599, USA*
[2]*Department of Marine Sciences, University of North Carolina at Chapel Hill, Chapel Hill, North Carolina 27599, USA*

We present an experimental study of single porous spheres settling in a near two-layer ambient density fluid. Data are compared with a first-principle model based on diffusive processes. The model correctly predicts accelerations of the sphere but does not capture the retention time at the density transition quantitatively. Entrainment of lighter fluid through a shell encapsulating the sphere is included in this model empirically. With this parametrization, which exhibits a power law dependence on Reynolds numbers, retention times are accurately captured. Extrapolating from our experimental data, model predictions are presented. © *2013 AIP Publishing LLC*. [http://dx.doi.org/10.1063/1.4819407]

Marine snow, aggregates composed of phytoplankton, fecal pellets, sediment, detritus, and other material, play an important role in the carbon flux to the deep ocean.[1,2] These aggregates range from approximately 100 μm to a few centimeters in size, and are often extremely porous (>99%).[3,4] Field observations have revealed that aggregates often accumulate in thin layers associated with sharp vertical density gradients in the ocean.[1,2] By acting as hotspots for bacterial degradation and zooplankton grazing,[3,4] these layers can affect the vertical redistribution of carbon in the water. Thus, understanding the interplay between stratification and increased aggregate accumulation may be important for accurate modeling of the vertical carbon flux in the ocean.

A first step in this direction is the understanding of settling dynamics of a single porous particle through sharp density gradients. Previous studies have explored the settling of solid non-porous particles in this situation. These studies have shown how fluid entrained from the upper regions causes a particle to slow down significantly when entering lower regions of denser fluid.[5–9] With porous particles, diffusion of the stratifying agent (e.g., salt) can add an extra physical mechanism affecting settling.[10] In some cases, the initial combined density of the solid porous medium and buoyant upper fluid may even be less than that of the lower fluid. Hence, the stratifying agent must diffuse into the pores to increase the particle's overall density in order for it to settle into the lower fluid.

In this paper, we show that a complete understanding of the settling behavior of a porous particle through a sharp density gradient requires modeling of both diffusion and entrainment mechanisms. We first present results from laboratory experiments with single porous spheres in salt-stratified, near two-layer fluids. The experimental data are then compared to a first-principle mathematical model for a porous sphere settling under diffusion. The need to account for entrainment clearly emerges from this comparison. We restore good agreement by a simple adjustment to the first-principle model. Entrained fluid is modeled as an additional shell around the sphere, augmenting the region where diffusion is the main mechanism for settling dynamics. Parametrization of the shell thickness

---

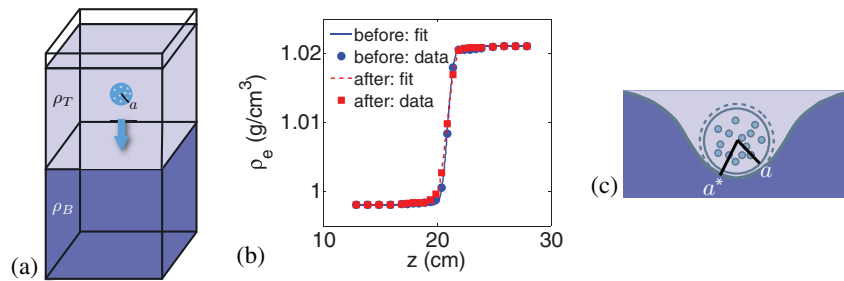a)khatri@email.unc.edu

25, 081701-1

FIG. 1. (a) Schematic of the near two-layer experiments: ρ_T top layer density, ρ_B bottom layer density, and a radius of settling porous sphere. (b) Density profile from temperature and conductivity measurements, before and after the set of experiments: data and error function fits with parameters z_c and t^*. (c) Schematic of entrainment by a settling sphere: radius a is augmented by a shell of upper layer fluid for a cumulative radius a^*.

is then explored as a function of the Reynolds number, which offers insight on different regimes depending on the physical parameters of the system.

Experimental methods: Porous spheres made of 1% agarose, using the methodology of Kiørboe *et al.*,[11] were used as a proxy for marine snow. By using laboratory manufactured spheres with properties similar to marine aggregates, we can eliminate uncertainties caused by irregular shape and nonuniform composition. The radii range from 0.0428 to 0.0943 cm.

Experiments were conducted in a $27.8 \times 27.8 \times 59.8$ cm^3 acrylic tank. Two different sets of experiments were performed. Settling of eight porous spheres was observed in homogenous water and in stratified water with a near two-layer density profile (Figure 1(a)). NaCl salt was used as the stratifying agent in deionized water. The densities of the homogenous tanks and of the two layers in the stratified tank were measured using a density meter (DMA 35, Anton Paar). To achieve a sharp stratification, bottom layer saltwater, with density $\rho_B = 1.021$ g/cm^3, was poured initially in the tank. Top layer fresh water, with density $\rho_T = 0.998$ g/cm^3, was then slowly added through a sponge diffuser, which minimized mixing of the two fluids. Both before and after the two-layer experiments, the temperature and conductivity were profiled with a conductivity probe (MSCTI Model 125, Precision Measurement Engineering, Inc.). A density profile was calculated from these measurements using the Gibbs-SeaWater Oceanographic Toolbox,[12] correcting linearly to agree with measured values of ρ_T and ρ_B. The density profiles before and after the two-layer settling experiments are shown in Figure 1(b).

Once the tank was filled, a 2.3 cm thick lid was submerged approximately 2 cm below the surface of the water. The lid served the purpose of both preventing free surface effects and guiding the sphere into an initial position at the center of a tank through a 4 mm diameter hole. Prior to each experiment, an image of each sphere was taken on a millimeter square grid for size measurement with a digital microscope (26700–300, Aven Inc.). For all experiments conducted, the sphere was soaked in top layer fluid before being released by pipette in the water column. The spheres were collected at the end of each set of experiments, and reused throughout.

A monochrome camera (Pike F-100B, Allied Vision Technologies) with computer imaging acquisition software (StreamPix, NorPix, Inc.) was used to image each sphere as it settled. Two light emitting diode panels were placed on the side walls of the tank during the experiments. Images with a field of view of 41.75×41.75 cm^2 and a resolution of 1 megapixel were taken at a fixed frame rate of 8 fps. At the end of each set of experiments, an image of a ruler in the center of the tank was used to calibrate pixels to centimeters. Images were processed using MATLAB to extract depth versus time plots for each sphere. The settling velocity as a function of time was then computed from the depth data using a finite difference method (following Anderssen and Hoog,[13] with $r = 8$).

Using the same methodology, homogenous ambient fluid experiments at five densities (0.998 g/cm^3, 1.010 g/cm^3, 1.021 g/cm^3, 1.030 g/cm^3, 1.041 g/cm^3) were conducted in order to assess the porosity (ratio of pore to total volume), P, and the density of the solid matrix of the agarose, ρ_s, of each sphere. Trials were repeated three times and imaged at 16 fps. An intermediate time interval of $\simeq 40$ s in which the sphere appeared to maintain constant terminal velocity was

selected to compute the average speed of each sphere in each experiment (by linear fit to the depth time-history). From the terminal velocity in each experiment, the density of the aggregate was then computed according to the Stokes drag law. (Empirical drag laws, for nonzero Reynolds numbers and for corrections due to wall drag, were tested and found to make no significant difference.) In total, 15 corresponding values of fluid density and aggregate density were assembled for each sphere; these data were linearly regressed to compute the porosity P and solid density ρ_s for each individual sphere. Additionally, data for all spheres were regressed to give a collective porosity and solid density, P^M and ρ_s^M. Different spheres had slightly varying porosity, ranging between 0.985 and 0.996, and solid density, ranging between 1.3 g/cm^3 and 1.6 g/cm^3, while collectively $P^M = 0.991 \pm 0.006$ and $\rho_s^M = 1.3 \pm 0.6$ g/cm^3. Values given throughout represent mean $\pm 95\%$ confidence interval. Even though the confidence intervals for the solid densities appear large, errors in ρ_s cancel (leaving the porosity and homogeneous terminal velocities as the only sources of error) when used in the mathematical model described next. Note that in the above parametric range the initial effective density of all spheres is less than that of the bottom ambient fluid.

Mathematical model: We develop a model for the two-layer experiment presented above (see Figure 1). A full mathematical description would require solving the Navier-Stokes equations for the ambient fluid motion, coupled to an advection-diffusion equation for the stratifying agent and to the motion of the sphere through unsteady boundary conditions. The motion of the sphere would have to be solved simultaneously according to the corresponding stresses from the fluid. Even for a single sphere, this is a challenging problem which can only be tackled through a fairly intensive computational effort. Therefore, we make simplifying assumptions, partially supported by the experimental data, to derive a model that can be quantitatively accurate yet simple enough to be thoroughly investigated analytically, e.g., for parametric dependence. Ultimately, the extent to which the model is relevant, even when stretching its applicability beyond regimes that satisfy the underlying hypotheses, is born out of the comparison of model solutions with experimental data.

Our first set of hypotheses concerns the physics of the viscous drag on the settling sphere. We assume viscous dominated regimes so that the Navier-Stokes equations simplify to their Stokes limit. Accordingly, inertia of both the ambient fluid and the settling sphere is neglected. Further, a no slip boundary condition is assumed on the entire surface of the sphere, as opposed to just on the solid portion, resulting in the use of the Stokes drag law as the viscous drag force. The next set of hypotheses address the diffusion processes of the stratifying agent (NaCl). Specifically, we assume that the total time of the experiment is short enough so that diffusion does not significantly alter the stratification of the ambient fluid during settling. However, the motion of the sphere in regions where significant diffusive mass exchange occurs is assumed to be sufficiently slow so as to not require accurate modeling of advection effects. Further, the length scales of gradients in the density stratification are assumed to be large compared to the radii of the settling spheres. These assumptions can be summarized by the nondimensional relations: Re $\equiv a U_T \rho_T / \mu \ll 1$, $a U_T / T_d \leq O(1)$, $\kappa/(U_e L_e) + \kappa H/(\bar{U} L_e^2) \ll 1$, $a U_e/\kappa \ll L_e/a$, and $a/L_e \ll 1$. Here, a is the sphere radius, H is the total tank height, L_e is the interfacial layer length scale, U_e is the average speed in this region, U_T is the terminal velocity in the top layer, $\bar{U}$ is the average of the top and bottom terminal velocities, ρ_T is the top layer fluid density, T_d is the deceleration time from U_T to near zero velocity as approaching the interface, μ and κ are the dynamic viscosity of water and diffusivity of NaCl in water, respectively, both assumed to be constant ($\mu = 0.01$ g/cm/s and $\kappa = 1.5 \times 10^{-5}$ cm^2/s). By comparing the time of diffusion into the sphere (accounting for the spherical geometry) with the time to settle through the layer with instantaneous density equilibration, these nondimensional relations single out a threshold radius which can be expected to play a role in the dynamics, $a_c^4 = 9\pi^2 L_e \mu \kappa/((1-P)(2\rho_s - (\rho_T + \rho_B))g)$, with $g = 980.7$ cm/s^2 denoting the gravitational acceleration.

Under our modeling assumptions, the settling velocity, U, of the sphere is given by the balance of Stokes' drag (neglecting permeability effects[14]) and buoyancy,

$$6\pi\mu a \frac{dZ}{dt} \equiv 6\pi\mu a U = -g\rho_e(Z(t))V + gM_{\text{sph}}(t), \tag{1}$$

where $\rho_e(z)$ is the ambient fluid density, $z = Z(t)$ is the sphere center depth, and V is the sphere volume. The mass of the sphere, $M_{\mathrm{sph}}(t)$, is dependent on the porosity of the sphere P and solid density ρ_s, $M_{\mathrm{sph}}(t) = P'V\rho_s + PM_{\mathrm{fl}}(t)$, where $P' = (1 - P)$. Time dependence enters through the mass of the fluid portion of the sphere, $M_{\mathrm{fl}}(t)$. This mass is affected by salt diffusivity. The diffusion equation is solved for the salinity within the sphere (using κ) with a time dependent Dirichlet boundary condition, set by the salt concentration in the ambient fluid at the sphere center depth $Z(t)$. This is equivalent to assuming that the ambient fluid is a "heat bath," consistently with the small sphere assumption. This boundary condition couples Eq. (1) with the diffusion equation, whose analytical solution (e.g., by Laplace transform) then results in a nonlinear integro-differential equation for the depth of the sphere $Z(t)$,

$$6\pi\mu a \frac{dZ}{dt} = -g\rho_e V + gP'V\rho_s + gP\left(V\rho_e + \sum_{n=1}^{\infty} A_n \int_0^t e^{\kappa k_n^2(\tau - t)}\frac{d\rho_e}{d\tau}\,d\tau\right), \qquad (2)$$

where $A_n = -8a^2/(nk_n)$, $k_n = n\pi/a$, and $V = (4/3)\pi a^3$. Here, we assume that the initial depth of the sphere is at the origin, $Z(0) = 0$, and the initial fluid density within the sphere is equal to the ambient fluid density, $\rho_o = \rho_e(Z(0)) = \rho_e(0)$. This equation for the depth of the sphere constitutes the simplest ("first-principle") form of our model. It has reduced the original coupled system of partial and ordinary differential equations for the fluid and porous medium interactions to a fairly simple integro-differential equation. In general, this equation can be solved for $Z(t)$ rather efficiently with minimal numerical assistance for any assigned ambient stratification. In fact, for the special case of a linear stratification it can even be solved in closed form using a Laplace transform. Details of solution methods for both the general and linear cases, as well as convergence tests we have performed to rule out any numerical artifact in our integration schemes, will be presented in future work.

A refinement of the model, which we will refer to as "parametrized," includes the entrainment of ambient fluid from the top layer into the bottom layer due to the sphere motion.[5–9] In our experiments this leads to rather complex dynamics; to make progress, we parametrize it here in the simplest possible way. To this extent, we assume that the entrained fluid is effectively enclosed in a shell region around the settling sphere, thus augmenting the radius of the fluid portion of the porous region to a cumulative effective radius $a^* \geq a$, see Figure 1(c). This is a coarse simplification which possibly neglects important dynamics observed in our solid sphere experiments due to fluid advection. For instance, leakage of entrained fluid through a trailing stem is observed in experiments with solid spheres.[6,8,9] On the other hand, a^* is the only adjustable parameter in a theory that has thus far been based on first principles. We stress that our model of the entrained shell affects the diffusion and buoyancy components of the dynamics, leaving the viscous drag untouched. Thus, Eq. (2) is adjusted to reflect the entrained contribution, which results in

$$6\pi\mu a \frac{dZ}{dt} = -g\rho_e V^* + gP'V\rho_s + g\left((V^* - P'V)\rho_e + \sum_{n=1}^{\infty} A_n^* \int_0^t e^{\kappa k_n^{*2}(\tau - t)}\frac{d\rho_e}{d\tau}\,d\tau\right), \qquad (3)$$

where $A_n^* = \frac{(-1)^n 8\pi}{k_n^{*3}}(P'(k_n^* a\cos(k_n^* a) - \sin(k_n^* a))) - \frac{8\pi a^*}{k_n^{*2}}$, $k_n^* = \frac{n\pi}{a^*}$, and $V^* = \frac{4}{3}\pi(a^*)^3$. Ultimately, the effectiveness of this parametrized model needs to be assessed with respect to the experiments, as discussed next.

Comparison with experiments and discussion: We present results from one set of experiments in a near two-layer ambient fluid with $\rho_T = 0.998$ g/cm^3 and $\rho_B = 1.021$ g/cm^3. The density profiles before and after the experiments are shown in Figure 1(b). We have fit solutions of the diffusion equation in the form $\rho_e(z) = \frac{\rho_B - \rho_T}{2}(1 + \mathrm{erf}(\frac{z - z_c}{\sqrt{4\kappa t^*}})) + \rho_T$ to these data by adjusting two parameters, the center of the profile z_c, and the time of diffusion t^*. The density profile remained largely constant through the duration of the experiments. The error function fits are used for the background ambient density profile in the mathematical model (using the average values of the parameters, $z_c = 20.907$ cm and $t^* = 8814$ s).

Figure 2 shows the experimental data for one of the spheres settling in the two-layer ambient profile, as well as the corresponding solutions of the first-principle model (with no entrainment)
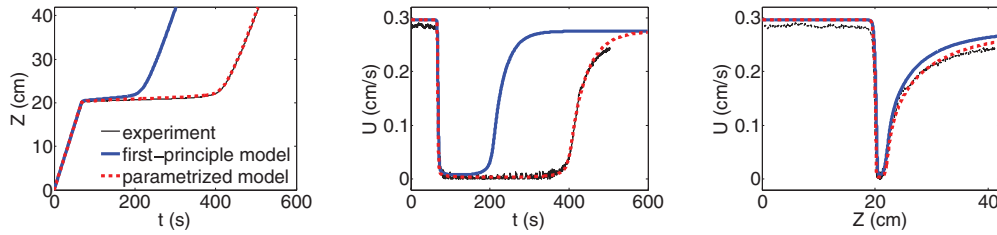
FIG. 2. Experimental data, first-principle model solution, and parametrized model solution (with $a^* = 1.18375a$) for an example of one sphere ($a = 0.0668 \pm 0.0004$ cm, $P = 0.991 \pm 0.002$, and $\rho_s = 1.3 \pm 0.3$ g/cm^3) settling in the two-layer ambient density profile shown in Figure 1(b): (a) depth vs. time, (b) settling velocity vs. time, and (c) settling velocity vs. depth.

and the parametrized model (with entrainment). A few remarks are in order. First, the terminal velocities in both top and bottom layers are captured accurately by the first-principle model without any need for adjustable parameters (Figure 2(b)). The slight offset in the top layer region is due to error in the terminal velocity measurements of the homogeneous settling control experiments (recall that the top terminal velocity in the model is not fitted to the stratified experiment), while the slow-down towards late times is due to proximity to the tank's floor. Next, the velocity versus depth predicted by the first-principle model also compares favorably with the data (Figure 2(c)). However, this agreement completely masks the large discrepancy in retention time observable in the velocity versus time plot (Figure 2(b)), which shows that the duration of the near-zero velocity transition is almost twice as long in the experiment as compared to the first-principle model. Note that this model still accurately captures the deceleration and the reacceleration phases of the time-history. Further, we plot the parametrized model solution with entrainment shell thickness a^* chosen as described below. As the comparison shows, this model is able to capture the retention of the sphere at the interface between layers, *without* altering the agreement of velocity through the acceleration phases. (Alternative parametrization strategies to capture the longer retention time, e.g., by adjusting diffusivity, or altering the drag law,[7] were tested but all resulted in poor agreement between model and experimental acceleration phases.)

Figure 3 presents time histories of experimental settling velocities and their counterpart from model solutions for increasing sphere radii. The first-principle model underpredicts the retention time of the sphere at the density interface. This disagreement is more pronounced for smaller spheres and decreases with increasing radius. We quantify the time delay for each sphere caused by the sharp density gradient using two metrics, which we term the settling time, T_s, and the enhanced settling time, T_{es}. The first is defined as the time it takes the sphere to descend through a fixed depth of 20 cm centered at $z = z_c$. This 20 cm extent is large enough to include the stratified region, yet small enough to avoid top and bottom boundary effects. The enhanced settling time T_{es} is defined as the difference between T_s and the reference time computed for traversing the same 20 cm interval in the limit of infinite salt diffusivity, whereby the density of the fluid within the sphere adjusts instantaneously to the ambient fluid density. Thus, T_{es} gives a measure of the delay due to finite
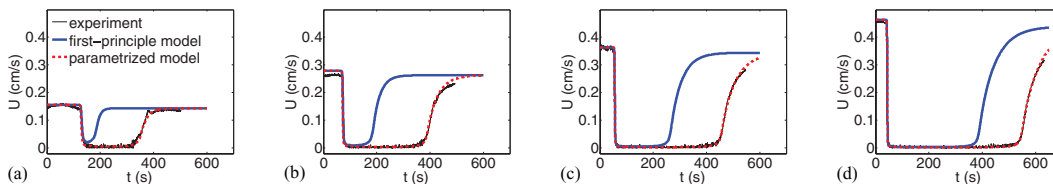

FIG. 3. Settling velocity vs. time (experimental data and first-principle and parametrized model solutions) for varying size spheres: (a) $a = 0.0428 \pm 0.0003$ cm ($P = 0.987 \pm 0.008$ and $\rho_s = 1.3 \pm 0.6$ g/cm^3), (b) $a = 0.0625 \pm 0.0003$ cm ($P = 0.992 \pm 0.002$ and $\rho_s = 1.4 \pm 0.3$ g/cm^3), (c) $a = 0.0784 \pm 0.0004$ cm ($P = 0.994 \pm 0.001$ and $\rho_s = 1.4 \pm 0.2$ g/cm^3), and (d) $a = 0.0943 \pm 0.0006$ cm ($P = 0.995 \pm 0.001$ and $\rho_s = 1.4 \pm 0.3$ g/cm^3). (Corresponding $a^* = (1 + \epsilon)a$ values are reported in Figure 4(b).)
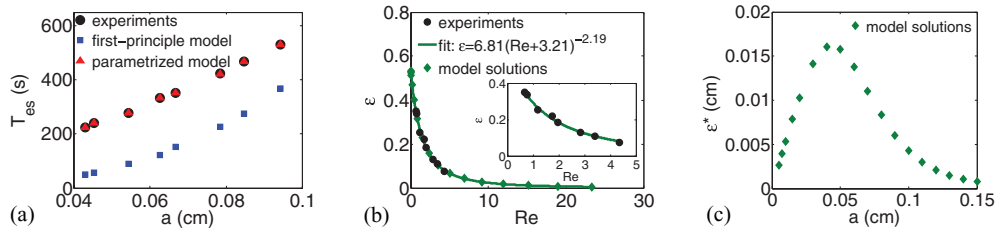
FIG. 4. (a) Enhanced settling time T_{es} vs. a for a set of spheres settling in the ambient density profile of Figure 1(b). Times from experimental data and the first-principle and parametrized models are shown. (b) Empirical parameter ϵ as function of Re (from top layer terminal velocity), shown as circles. Curves show functional fit and extrapolation. Diamonds correspond to values used in the models. (c) Parameter ϵ^* as function of a used in model solutions for Figure 5 below.

diffusivity. (Whenever necessary to avoid confusion, we use superscript labels $T_{s,es}^{exp}$, $T_{s,es}^{fp}$, and $T_{s,es}^*$ to identify the settling and enhanced settling times for the experiments, first-principle model, and parametrized model, respectively.) Figure 4(a) summarizes the results for T_{es}, showing comparisons between experimental data and the model predictions for the different spheres. We hypothesize that the difference between the first-principle model and data can be explained by the added effect of entrainment. By incorporating an entrained shell whose thickness relative to a decreases as the sphere radius increases (Figure 4(b)), good agreement can be recovered between the model and experiments (Figure 4(a)).

To describe the entrainment shell, we introduce the nondimensional parameter ϵ through $a^* = (1 + \epsilon)a$, where a^* is the radius of the outer boundary of the shell, see Figure 1(c). This parameter is optimized so T_{es}^* agrees with T_{es}^{exp} within half a second, as shown in Figure 4(a), thus giving a range of ϵ values for the experiments. These are plotted versus the Reynolds numbers for each sphere in Figure 4(b). A functional fit to these data is extrapolated below to small Re and above up to Re = 25, and the resulting law is used in a set of model solutions with varying radii. Figure 4(c) presents the $\epsilon^* \equiv \epsilon a$ shell thickness values versus radii which are used in the parametrized model (these solutions are shown in Figure 5). Note that $\epsilon^* \to 0$ as $a \to 0$ is physically reasonable for fluid entrained by small radii spheres. An entrainment shell parametrization to define an empirical drag law has been used in previous literature; however, we remark that the dependence of shell thickness on sphere radius and velocity found here seems novel, and is in contrast with a constant value set uniquely by viscosity and ambient fluid stratification.[7] Such a constant thickness used in our model would lead to far larger retention times than those measured in our experiments, though the setup of towed, as opposed to free-falling, solid spheres and linear stratification used in Yick *et al.*[7] is different from ours and might partially account for the discrepancy.

Times T_s and T_{es} for the models, as defined above, with and without the parametrized entrainment shell contribution, are displayed in Figures 5(a) and 5(b). In particular for the first-principle model solutions, we fit the functional forms (with appropriate dimensional interpretation for the constants as a is in centimeters and T is in seconds)

$$T_s^{fp} = (2.17 \times 10^4)a^{1.86} + (2.98 \times 10^{-1})a^{-2.00} \quad \text{and} \quad T_{es}^{fp} = (2.18 \times 10^4)a^{1.86} \tag{4}$$

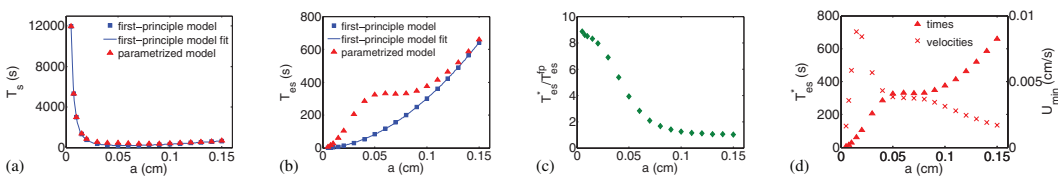

FIG. 5. Model solutions: (a) and (b) Settling time T_s and enhanced setting time T_{es} for the radii a shown in Figure 4(c) with fixed $P^M = 0.991$ and $\rho_s^M = 1.3$ g/cm^3 (functional fits given in Eq. (4)). (c) Enhanced settling time ratio T_{es}^*/T_{es}^{fp} vs. a. (d) T_{es}^* and minimum velocity U_{min} vs. a.

for the dependence on the radius a. These power laws express scalings that bring forth the role of diffusion in different regimes. For small spheres, with all parameters other than radii fixed, diffusion can be expected to keep the fluid density within the sphere matched to that of the local ambient fluid. A time scaling proportional to $1/a^2$ as $a \to 0$ emerges in this case from Eq. (2), and can be seen directly by how the radius a enters in this force balance. In the opposite limit of large spheres, for an initial density of the sphere which is buoyant with respect to the lower fluid density, the time of diffusion, required for the sphere to continue to settle in the denser fluid, is proportional to a^2. This agrees with the trends exhibited by the functions in Eq. (4).

Entrainment, and the complex dynamics that it can trigger,[6] can be expected to affect these time scales. Figure 5(c) shows the ratio of the two enhanced settling times with and without parametrized entrainment. The plot reinforces the trend of the increased role played by entrained shells for smaller spheres, which is noticeable in Figure 3. Through Figure 5(d), we observe that the change in curvature in T_{es}^* as a function of a seems to correlate with the radius at which the minimum velocity U_{min} dips towards zero after a short plateau at intermediate a's. This range of values roughly agrees with the estimate provided by the critical radius a_c mentioned above ($a_c = 0.046$ cm in this case).

We have shown that the retention time of porous particles at sharp density gradients, as in the near two-layer study presented here, depends on both entrainment of stratified fluid by settling particles and diffusion of the stratifying agent through both entrained and pore fluid. While our study is focused on isolating the fundamental mechanisms in a controlled lab environment with a single settling particle, the phenomena we identified may play a relevant role in the formation of marine aggregate layers. Persistence of layers in equilibrium and their levels of aggregate accumulation could depend heavily on the balance between the effects studied here. Further studies are being pursued to improve on the current model by first principle parametrization of entrainment.

[1] S. MacIntyre, A. L. Alldredge, and C. C. Gotschalk, "Accumulation of marine snow at density discontinuities in the water column," Limnol. Oceanogr. **40**, 449–468 (1995).

[2] A. L. Alldredge, T. J. Cowles, S. MacIntyre, J. E. B. Rines, P. L. Donaghay, C. F. Greenlaw, D. V. Holliday, M. M. Dekshenieks, J. M. Sullivan, and J. R. V. Zaneveld, "Occurrence and mechanisms of formation of a dramatic thin layer of marine snow in a shallow Pacific fjord," Mar. Ecol.: Prog. Ser. **233**, 1–12 (2002).

[3] A. L. Alldredge and M. W. Silver, "Characteristics, dynamics and significance of marine snow," Prog. Oceanogr. **20**, 41–82 (1988).

[4] A. B. Burd and G. A. Jackson, "Particle aggregation," Annu. Rev. Marine Sci. **1**, 65–90 (2009).

[5] A. N. Srdić-Mitrović, N. A. Mohamed, and H. J. S. Fernando, "Gravitational settling of particles through density interfaces," J. Fluid Mech. **381**, 175–198 (1999).

[6] N. Abaid, D. Adalsteinsson, A. Agyapong, and R. M. McLaughlin, "An internal splash: Levitation of falling spheres in stratified fluids," Phys. Fluids **16**, 1567–1580 (2004).

[7] K. Y. Yick, C. R. Torres, T. Peacock, and R. Stocker, "Enhanced drag of a sphere settling in a stratified fluid at small Reynolds numbers," J. Fluid Mech. **632**, 49–68 (2009).

[8] R. Camassa, C. Falcon, J. Lin, R. M. McLaughlin, and R. Parker, "Prolonged residence times for particles settling through stratified miscible fluids in the Stokes regime," Phys. Fluids **21**, 031702-1–031702-4 (2009).

[9] R. Camassa, C. Falcon, J. Lin, R. M. McLaughlin, and N. Mykins, "A first-principle predictive theory for a sphere falling through sharply stratified fluid at low Reynolds numbers," J. Fluid Mech. **664**, 436–465 (2010).

[10] K. Kindler, A. Khalili, and R. Stocker, "Diffusion-limited retention of porous particles at density interfaces," Proc. Natl. Acad. Sci. U.S.A. **107**, 22163–22168 (2010).

[11] T. Kiørboe, H.-P. Grossart, H. Ploug, and K. Tang, "Mechanisms and rates of bacterial colonization of sinking aggregates," Appl. Environ. Microbiol. **68**, 3996–4006 (2002).

[12] T. J. McDougall and P. M. Barker, "Getting started with TEOS-10 and the Gibbs Seawater (GSW) Oceanographic Toolbox," SCOR/IAPSO WG127, 2011.

[13] R. S. Anderssen and F. R. de Hoog, "Finite difference methods for the numerical differentiation of non-exact data," Computing **33**, 259–267 (1984).

[14] B. S. Padmavathi, T. Amaranath, and S. D. Nigam, "Stokes flow past a porous sphere using Brinkman's model," Z. Angew. Math. Phys. **44**, 929–939 (1993).